# Hybrid Fast Fourier Transform–plane wave based near-field far-field transformation for "body of revolution" antenna measurement grids

C. H. Schmidt,[1] T. A. Laitinen,[2] and T. F. Eibert[1]

Received 3 January 2011; revised 28 June 2011; accepted 18 July 2011; published 20 October 2011.

[1] Near-field measurement and transformation techniques are widely applied to characterize radiation patterns of antennas. Spherical and cylindrical near-field measurements have been researched extensively and various techniques with different probe compensation capabilities and complexities exist. Among those techniques applicable for (almost) arbitrary probes, the crucial computational efficiency has been achieved through the use of Fast Fourier Transform based preprocessing of the measurement data. It is shown in this paper that the Fast Fourier Transform based preprocessing can also be utilized in conjunction with the plane wave based fully probe-corrected near-field far-field transformation with low numerical complexity. The collection of probe signals is split into smaller subsets for individual orthogonal azimuthal Fourier modes by an Inverse Fast Fourier Transform. These smaller subsets can be transformed to the far field very efficiently with full probe correction. The technique presented in this paper is applicable for arbitrary "body of revolution" antenna measurement grids, including the important cases of cylindrical and spherical measurement grids. The "body of revolution" grids are rotationally symmetric around the $z$-axis and the probe signals must be available equidistantly in $\varphi$.

**Citation:** Schmidt, C. H., T. A. Laitinen, and T. F. Eibert (2011), Hybrid Fast Fourier Transform–plane wave based near-field far-field transformation for "body of revolution" antenna measurement grids, *Radio Sci.*, *46*, RS0E15, doi:10.1029/2010RS004640.

## 1. Introduction

[2] Near-field antenna measurements and near-field to far-field transformations have been a subject of extensive research efforts over the years [*Larsen*, 1977; *Yaghjian and Wittmann*, 1985; *Yaghjian*, 1986; *Hansen*, 2009]. Recently, probe pattern compensated near-field to far-field transformation techniques, known as probe correction techniques, have fascinated different researchers as evidenced, for example, by *Laitinen et al.* [2005], *Schmidt et al.* [2008], *Pogorzelski* [2008], and *Laitinen et al.* [2010]. These probe correction techniques are required to accurately determine the far field from probe signals gathered in the near field of the antenna under test (AUT) [*Yaghjian*, 1986].

[3] Until recently, the first-order probe correction technique [*Wacker*, 1974; *Jensen*, 1975], described in detail by *Hansen* [1988], has been the preferred technique for spherical near-field measurements due to its computational efficiency and stability. The application of this technique requires a specific probe to be used which has only first-order azimuthal variations in its pattern. Also scanning must occur on a rectangular $\varphi$-$\theta$ scan grid at a fixed measurement distance. Although being computationally powerful, the use of the first-order technique has been seen problematic in a few respects. In particular, the probe requirement imposed by the first-order technique has been considered a problem [*Laitinen et al.*, 2005], but also confining to a regular $\varphi$-$\theta$ grid and a fixed measurement distance may be unfavorable in some cases.

[4] Several probe correction techniques have been recently presented, allowing a full probe correction for probes possessing also zeroth-order or higher than first-order variations in their azimuthal pattern. Although providing simplifications in the probe requirements, these so-called high-order probe correction techniques [*Laitinen et al.*, 2005; *Laitinen*, 2008; *Pogorzelski*, 2008] require, similar to the first-order probe correction technique, the probe signals to be available on a regular $\varphi$-$\theta$ scan grid. These techniques have a higher computational complexity compared to the first-order probe correction technique.

[5] Plane wave based near-field far-field transformation techniques with full probe correction inspired by the Fast Multipole Method (FMM) [*Coifman et al.*, 1993] and Multilevel Fast Multipole Method (MLFMM) [*Chew et al.*, 2001] have been recently presented by *Schmidt et al.* [2008] and *Schmidt and Eibert* [2009]. Advantageously, these

[1]Lehrstuhl für Hochfrequenztechnik, Technische Universität München, Munich, Germany.
[2]Aalto University School of Electrical Engineering, Department of Radio Science and Engineering, Espoo, Finland.


0048-6604/11/2010RS004640

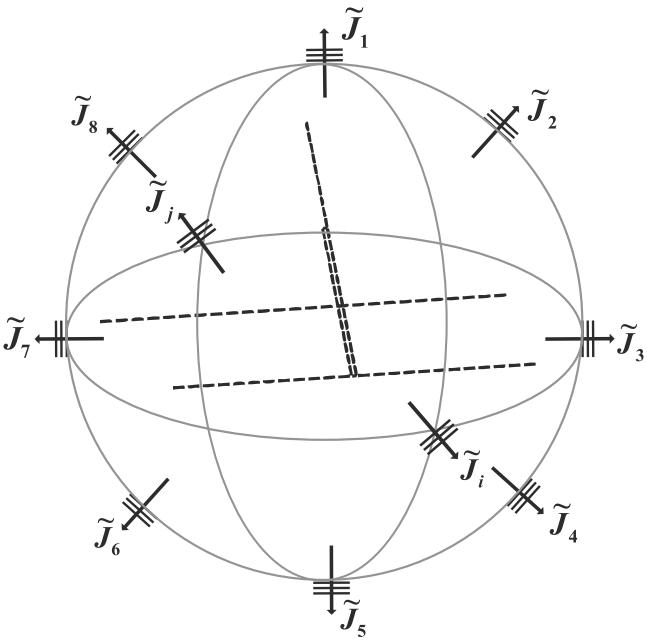


**Figure 1.** The *k*-space representation of AUT.

techniques are applicable to arbitrary and irregular measurement contours. Moreover, the computational complexity of the multilevel plane wave based technique [*Schmidt and Eibert*, 2009] is $O(N \log N)$ per iteration of the employed iterative linear equation solver, which is lower than that of the first-order probe correction technique. Hereby, $N$ refers to the number of measurement points. In terms of the computational complexity, the plane wave based multilevel transformation is superior to the other probe correction techniques presented so far. However, the plane wave expansion is an interpolatory representation of the AUT antenna pattern demanding a certain amount of oversampling for the interpolations to work. This does, however, not require to increase the measurement sample density and dependent on the chosen interpolations the oversampling of the internal AUT pattern representations can be very low. In contrast, the modal expansions are hierarchical orthogonal series expansions, where the individual modes can be processed independently and any sampling redundancy can be removed. Therefore, it is desirable to work with orthogonal expansions where possible.

[6] Recent work presented by *Schmidt et al.* [2010] has shown that the azimuthal Fourier mode expansion with Fast Fourier Transform preprocessing can be successfully utilized in conjunction with the single level plane wave based near-field far-field transformation [*Schmidt et al.*, 2008] to speed-up the computations for spherical near-field measurements at the cost of restriction to measurement grids equidistantly sampled in $\varphi$. The purpose of this work, as a continuation of the work presented by *Schmidt et al.* [2010], is to present and demonstrate the functionality of a low complexity near-field far-field transformation technique with full probe correction that is based on Fast Fourier Transform preprocessing and the multilevel plane wave based transformation algorithm. This technique is essentially similar to the work of *Schmidt et al.* [2010], but it is now employed with the multilevel transformation algorithm inspired by the MLFMM. The technique takes advantage of the orthogonality property of the azimuthal Fourier modes in the same manner as done in the first-order probe correction. Then, it exploits the low complexity plane wave based near-field transformation for the remaining computations. In this way, as compared to the work of *Schmidt and Eibert* [2009], a lower overall computation time is achieved and the computational complexity of the technique is not increased. It is, however, noted that the computational improvements are reached at the expense that arbitrary measurement contours are not applicable anymore. The exploitation of the orthogonality property of the azimuthal Fourier modes restricts the applicable measurement grids to those which are rotationally symmetric around the $z$-axis and where the probe signals are available equidistantly in $\varphi$ from 0° to

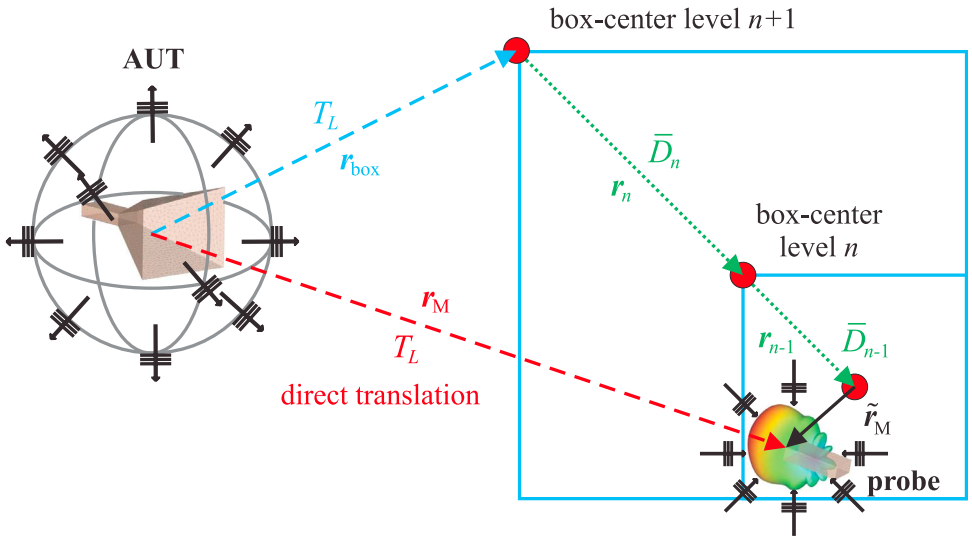


**Figure 2.** Plane wave processing in multilevel algorithm by translation and disaggregation/anterpolation.

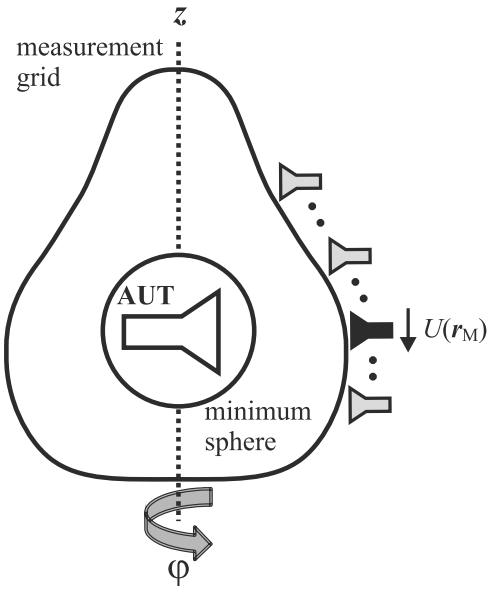


**Figure 3.** Measurement setup for "body of revolution" measurement grid.

$360° - \Delta\varphi$, where $\Delta\varphi$ is the $\varphi$ step. Hence, this new technique is applicable for "body of revolution" scan surfaces.

[7] Section 2 of this paper presents the theory of the technique. Section 3 describes the simulations, and section 4 describes the measurements for the validation of the technique. Conclusions are presented in section 5.

## 2. Theory

### 2.1. Plane Wave Based Near-Field Far-Field Transformation

[8] The plane wave based near-field far-field transformation algorithm [*Schmidt et al.*, 2008] describes the radiation behavior of the AUT by a set of plane waves $(\overline{\boldsymbol{I}} - \hat{k}\hat{k}) \cdot \tilde{\boldsymbol{J}}(\hat{k})$ propagating in all spatial directions as visualized in Figure 1. The probe signal

$$\boldsymbol{U}(\boldsymbol{r}_M) = -\mathrm{j}\frac{\omega\mu_0}{4\pi} \oiint T_L\left(\hat{k}, \hat{r}_M\right)\overline{\boldsymbol{P}}\left(\hat{k}, \boldsymbol{r}_M\right) \cdot \left(\overline{\boldsymbol{I}} - \hat{k}\hat{k}\right) \cdot \tilde{\boldsymbol{J}}\left(\hat{k}\right) \mathrm{d}\hat{k}^2 \quad (1)$$

at a measurement point $\boldsymbol{r}_M$ is obtained by translating the plane waves from the AUT to the field probe position by multiplication with the diagonal translation operator $T_L(\hat{k}, \hat{r}_M)$, known from FMM. $\omega$ is the angular frequency, $k$ the wave number and $\overline{\boldsymbol{I}}$ the unit dyad. The field probe influence is incorporated completely by multiplication of the translated plane waves with the probe correction coefficient $\overline{\boldsymbol{P}}(\hat{k}, \boldsymbol{r}_M)$ containing the far-field pattern of the field probe and the antenna factor relating the measured field strength to the probe output signal.

[9] For an efficient near-field processing of electrically large antennas, the transformation algorithm is extended in a multilevel fashion [*Schmidt and Eibert*, 2009] similar to the MLFMM, resulting in a reduced complexity of $O(N \log N)$. For this, the measurement points are grouped in a recursive box structure, and the plane wave spectrum is translated to the box centers of the highest level boxes only (see Figure 2) resulting in the plane wave spectrum

$$\tilde{\boldsymbol{J}}_N^{i_N}\left(\hat{k}\right) = T_L\left(\hat{k}, \hat{r}_{\mathrm{box}}\right)\left(\overline{\boldsymbol{I}} - \hat{k}\hat{k}\right) \cdot \tilde{\boldsymbol{J}}\left(\hat{k}\right). \quad (2)$$

The plane wave spectrum is then processed through the levels to the measurement points by a disaggregation and anterpolation procedure resulting in the plane wave spectrum

$$\tilde{\boldsymbol{J}}_n^{i_n}\left(\hat{k}\right) = \overline{\boldsymbol{D}}_n^{i_n}\left(\boldsymbol{k}, \boldsymbol{r}_n^{i_n}\right) \cdot \left(\overline{\boldsymbol{I}} - \hat{k}\hat{k}\right) \cdot \tilde{\boldsymbol{J}}_{n+1}^{i_{n+1}}\left(\hat{k}\right) \quad (3)$$

at the level $n$ boxes.

$$\overline{\boldsymbol{D}}_n^{i_n}\left(\boldsymbol{k}, \boldsymbol{r}_n^{i_n}\right) = \overline{\boldsymbol{V}}_n\left(\hat{k}\right)\mathrm{e}^{-\mathrm{j}\boldsymbol{r}_n^{i_n}\cdot\boldsymbol{k}} \quad (4)$$

is the combined disaggregation and anterpolation operator. Disaggregation is a simple phase shift from the box center

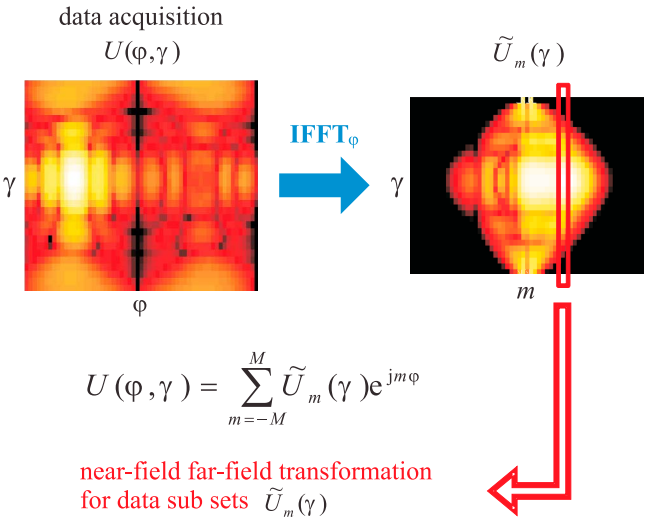


**Figure 4.** Work flow of hybrid near-field far-field transformation algorithm.

Electric dipole distribution synthesizing horn antenna

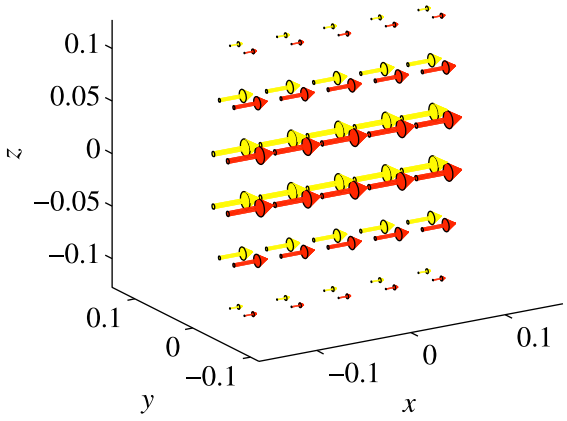


**Figure 5.** Electric dipole distribution synthesizing horn antenna at 3 GHz. The arrow thickness is representing the dipole magnitude, the color is representing the dipole phase.

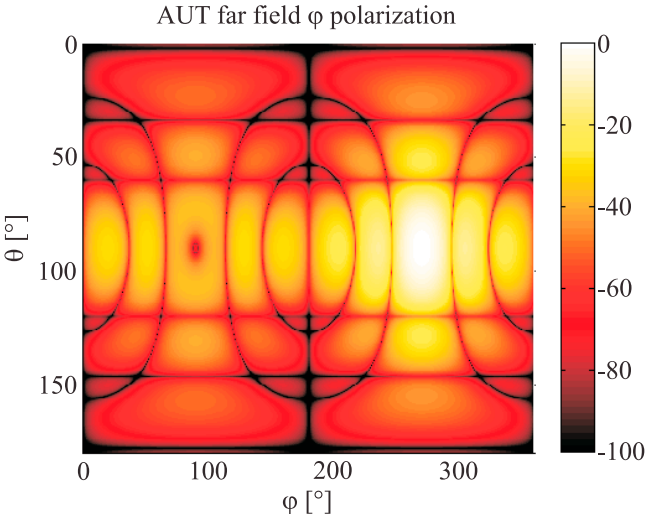


**Figure 6.** Reference far-field pattern of horn antenna synthesized by electric dipole distribution at 3 GHz, $\varphi$ polarization.

on level $n + 1$ to the box center on level $n$ or finally the measurement points. Anterpolation can be seen as adjoint operation to interpolation and reduces the sampling rate of the plane wave spectrum. The spectral content on the various levels is proportional to the size of the boxes being considered, just as the radiation pattern of an electrically large antenna has a higher spectral content than those of an electrically small antenna. Therefore it is possible to describe the plane wave spectrum on lower levels with less samples. This is the key point to obtain a reduced overall complexity of the algorithm. On the lowest level of the box structure the probe signal

$$\boldsymbol{U}(\boldsymbol{r}_{\mathrm{M}}) = -\mathrm{j}\frac{\omega\mu_0}{4\pi}\sum_{k_\varphi}\sum_{k_\theta} W_\theta^{k_\theta,L} W_\varphi^{L} \mathrm{e}^{-\mathrm{j}\tilde{\boldsymbol{r}}_{\mathrm{M}}\cdot\boldsymbol{k}} \overline{\boldsymbol{P}}\left(\hat{k}, \boldsymbol{r}_{\mathrm{M}}\right)\cdot\left(\overline{\boldsymbol{I}} - \hat{k}\hat{k}\right)\cdot\tilde{\boldsymbol{J}}_0^{i_0}\left(k_\varphi, k_\theta\right) \tag{5}$$

is obtained by evaluating the integrals using numerical quadrature. $W_\theta^{k_\theta,L}$ and $W_\varphi^{L}$ are the quadrature weights of the Gauß-Legendre quadrature [*Abramowitz and Stegun*, 1972] and $\mathrm{e}^{-\mathrm{j}\tilde{\boldsymbol{r}}_{\mathrm{M}}\cdot\boldsymbol{k}}$ is the final phase shift from the box center on the lowest level to the measurement point $\boldsymbol{r}_{\mathrm{M}}$. The probe correction is implemented on the lowest level for a minimum number of plane wave samples thus representing the low-pass behavior of typical near-field probes of small to medium size.

[10] The algorithm is implemented to utilize the iterative generalized minimum residual (GMRES) solver [*Saad*, 2003]. After an initialization step, where the measurement setup is preprocessed and translation and disaggregation operators are precomputed, the operations as described in (2)–(5) are carried out on the fly. This means that the operations are performed for groups of measurement points one after another and that a matrix equation is not setup explicitly.

### 2.2. Hybrid Technique for "Body of Revolution" Antenna Measurement Grids

[11] For "body of revolution" measurement grids, i.e. those grids which are rotationally symmetric around the $z$-axis (see Figure 3) and where the probe signals are available equidistantly in $\varphi$, it is possible to utilize the equidistant sampling of the antenna fields in $\varphi$ to expand the measured probe signals in azimuthal Fourier modes

$$\boldsymbol{U}(\varphi,\gamma) = \sum_{m=-M}^{M} \tilde{\boldsymbol{U}}_m(\gamma)\mathrm{e}^{\mathrm{j}m\varphi} \tag{6}$$

by an Inverse Fast Fourier Transform (IFFT). $\gamma$ is the second coordinate besides $\varphi$ which specifies the measurement grid; i.e. $\gamma = \theta$ for spherical measurements and $\gamma = z$ for cylindrical measurements. The amplitude is constant for a fixed $\gamma$ and the phase is varying according to $\mathrm{e}^{\mathrm{j}m\varphi}$.

[12] Due to the orthogonality property of the exponential function, it is possible to decouple the azimuthal Fourier modes of the measured probe signals into subsets $\tilde{\boldsymbol{U}}_m(\gamma)$.

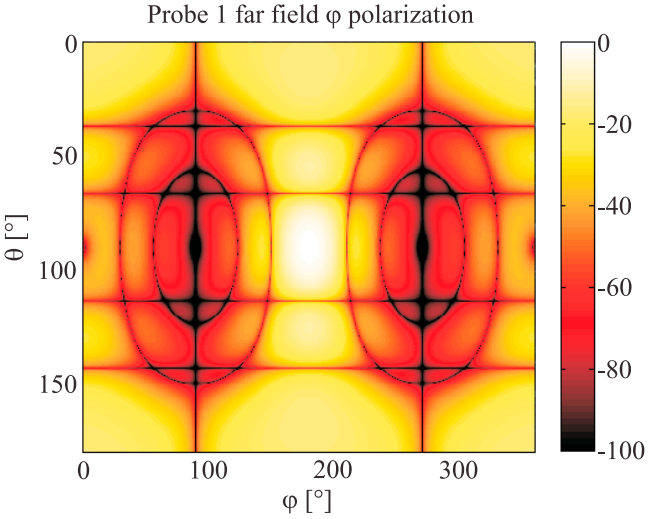


**Figure 7.** Far-field pattern of first probe synthesized by electric dipole distribution at 3 GHz, $\varphi$ polarization.

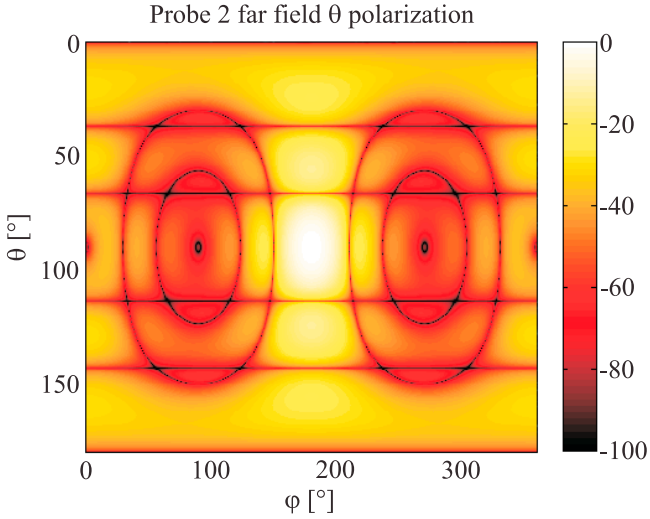


**Figure 8.** Far-field pattern of second probe synthesized by electric dipole distribution at 3 GHz, $\theta$ polarization.

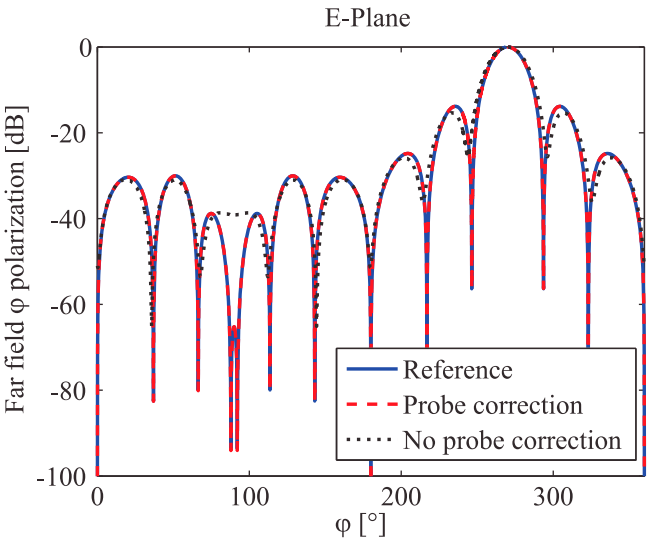


**Figure 9.** Transformed far-field pattern of horn antenna at 3 GHz with and without probe correction, spherical measurement $r$ = 0.5 m, E-plane cut, $\varphi$ polarization.

These subsets are then transformed to the far field independently (see Figure 4) by the plane wave based technique described in section 2.1. Due to the modal expansion, the $\varphi$-dependence of the probe signals is transformed into the $m$-dependence which is covered by considering the independent subsets. Now it is sufficient to setup the multilevel box structure for $\varphi = 0°$ only. The subsets thus contain only one $\gamma$-cut of measurement points. The drastically reduced number of measurement points in each subset results in a significant speed-up of the solution.

[13] Once all subsets have been transformed to the far field, the overall solution

$$\tilde{\boldsymbol{J}}\left(\hat{k}\right) = \sum_{m=-M}^{M} \tilde{\boldsymbol{J}}_m\left(\hat{k}\right) \mathrm{e}^{\mathrm{j}mk_\varphi} \tag{7}$$

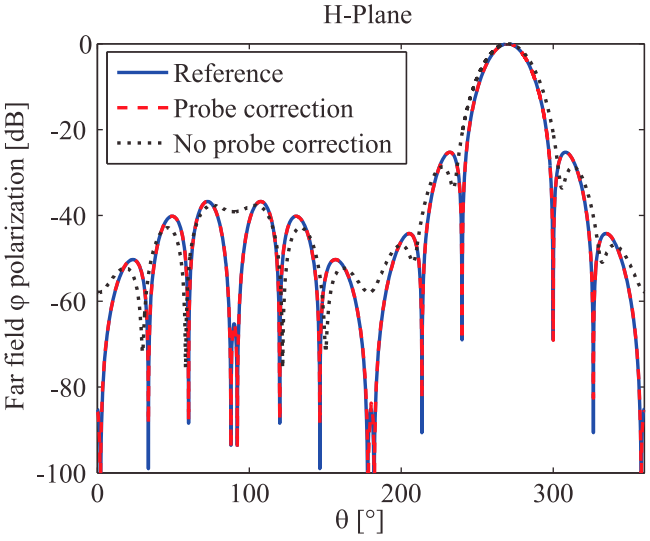


**Figure 10.** Transformed far-field pattern of horn antenna at 3 GHz with and without probe correction, spherical measurement $r$ = 0.5 m, H-plane cut, $\varphi$ polarization.

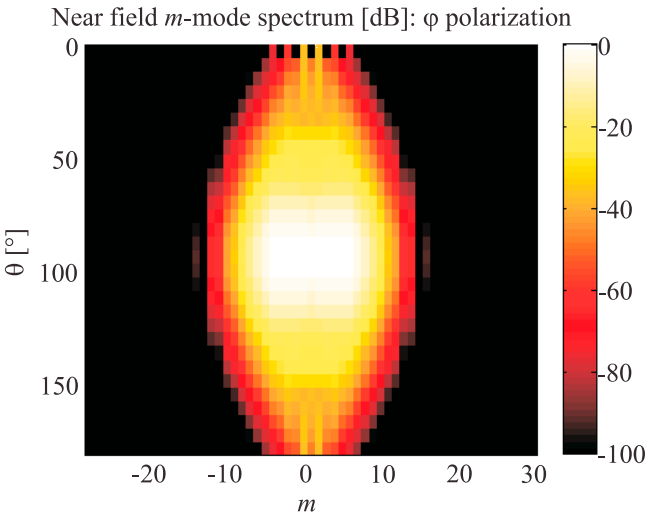


**Figure 11.** The $m$-mode spectrum of horn antenna at 3 GHz, spherical measurement $r$ = 0.5 m, $\varphi$ polarization.

is computed by superimposing all subset solutions $\tilde{\boldsymbol{J}}_m(\hat{k})$ with the appropriate phase factors.

[14] For certain bodies of revolution it might be possible that the related system matrix gets singular. In this case the singularity will be handled by the inherent regularization property of the GMRES solver.

## 3. Simulation Results

[15] The performance of the hybrid near-field far-field transformation is first demonstrated by means of synthetically generated near-field data in order to evaluate the performance without any measurement errors.

### 3.1. AUT, Probes, and Data Generation

[16] The AUT is a rectangular horn antenna which is synthesized by a distribution of electric dipoles placed in the antenna aperture as shown in Figure 5. The thickness of the

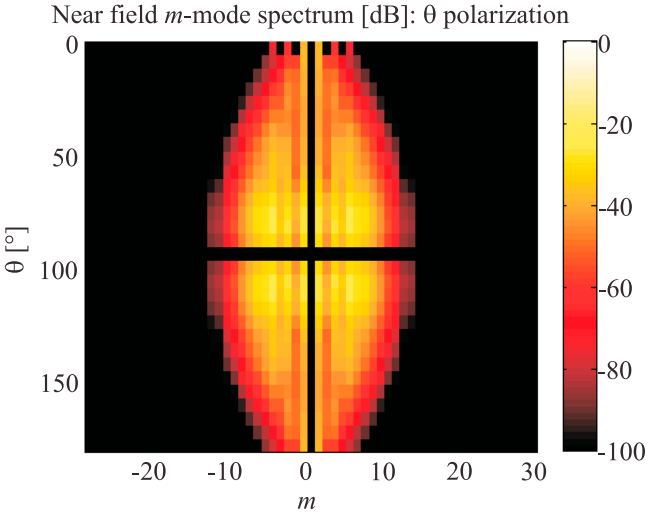


**Figure 12.** The $m$-mode spectrum of horn antenna at 3 GHz, spherical measurement $r$ = 0.5 m, $\theta$ polarization.

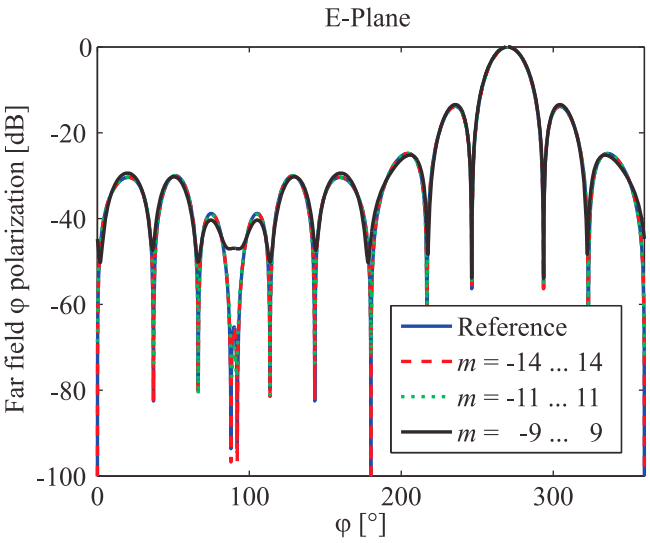


**Figure 13.** Transformed far-field pattern of horn antenna at 3 GHz for different $m$-index ranges, spherical measurement $r$ = 0.5 m, E-plane cut, $\varphi$ polarization.

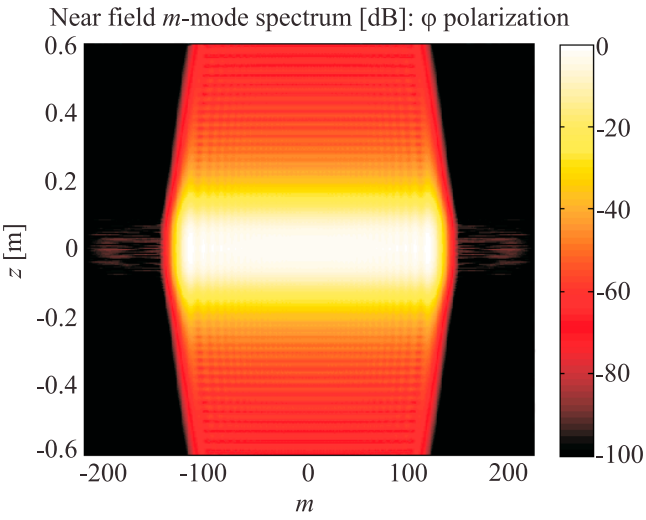


**Figure 15.** The $m$-mode spectrum of horn-like antenna at 60 GHz, cylindrical measurement $r$ = 1 m, $h$ = 1.2 m, $\varphi$ polarization.

arrow represents the dipole magnitude and the color represents the dipole phase. Two layers of dipoles are used, separated by $\lambda/4$ and having a 90° phase shift in order to minimize radiation in backward direction. Electric near fields are now computed by evaluating the dyadic Green's function of free space at the observation point for each dipole with its individual magnitude, phase, and orientation and by superimposing all contributions. The reference far field pattern is generated analogous by computing electric field values on a sphere in far field distance of the AUT. The reference far field pattern of the horn antenna is shown in Figure 6 for the $\varphi$ polarization.

[17] In order to consider the effects of the field probes used in near-field antenna measurements, the probes are synthesized by electric dipole distributions as well. The fields of the AUT are computed at the positions of the probe dipoles and are weighted by their individual magnitude, phase, and orientation. The probe signal is obtained as superposition of all probe dipole signals.

### 3.2. Spherical Near-Field Measurements

[18] For the first example, the probe correction capabilities of the hybrid near-field far-field transformation algorithm shall be demonstrated and therefore two probe antennas of similar dimensions as the AUT are chosen in order to have probe patterns with considerable nulls to pronounce the probe effects on the measurement. The probe far-field patterns are shown in Figures 7 and 8 for the dominant polarization components. Probe signals are computed at 3 GHz on a spherical grid with radius 0.5 m and 6°

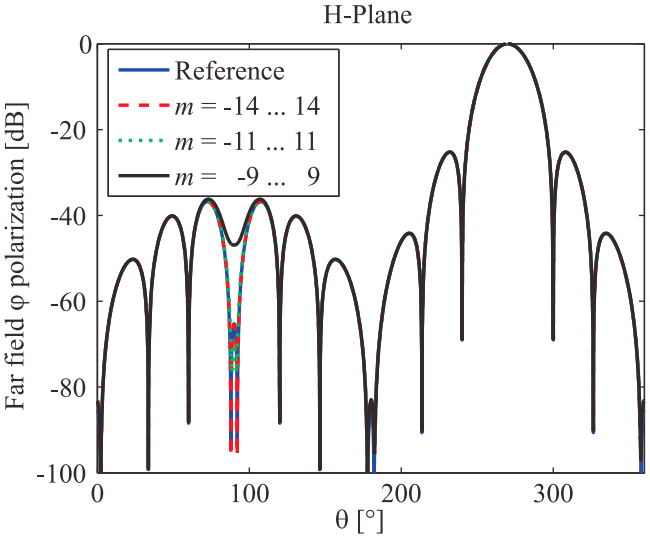


**Figure 14.** Transformed far-field pattern of horn antenna at 3 GHz for different $m$-index ranges, spherical measurement $r$ = 0.5 m, H-plane cut, $\varphi$ polarization.

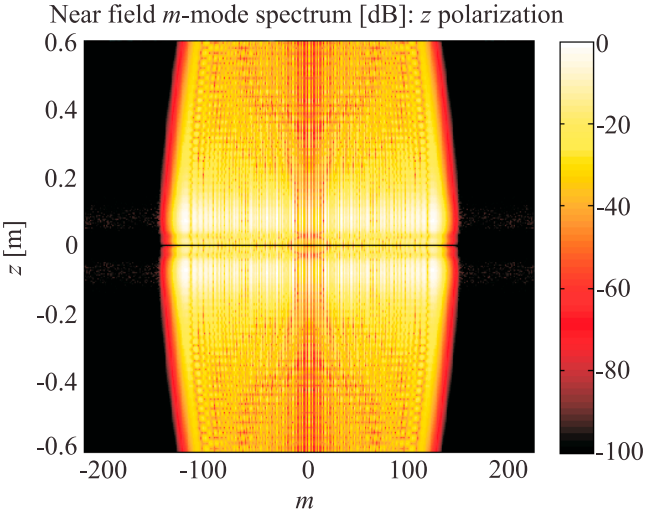


**Figure 16.** The $m$-mode spectrum of horn-like antenna at 60 GHz, cylindrical measurement $r$ = 1 m, $h$ = 1.2 m, $z$ polarization.

**Table 1.** Box Structure for Cylindrical Measurement Setup With Horn-Like Antenna

| Level | Box Side Length | Plane Wave Samples | Boxes |
|---|---|---|---|
| 0 | 0.01 m | 1 058 | 123 |
| 1 | 0.02 m | 2 888 | 63 |
| 2 | 0.04 m | 8 712 | 33 |
| 3 | 0.08 m | 154 568 | 18 |
| 4 | 0.16 m | 215 168 | 6 |

step size in $\varphi$ and $\theta$ resulting in 1 860 samples for each probe polarization. The problem has 880 unknowns according to the work of *Hansen* [1988]. In this measurement some oversampling was applied in order to investigate the transformation for different ranges of the $m$-indices. The spherical configuration is chosen to eliminate truncation errors while considering the probe correction capabilities. The hybrid transformation is carried out with and without probe correction. With probe correction, the far-field patterns of the probe antennas are considered in the transformation, without probe correction all plane wave contributions are superimposed uniformly without weighting according to a receiving characteristic of the probe. The transformed E- and H-plane far-field patterns are shown in Figures 9 and 10. The significant effects of the measurement probes, pronounced by the short measurement distance of 0.5 m, are obvious and can be successfully corrected by the near-field transformation algorithm including probe correction.

[19] In Figures 11 and 12 the $m$-mode spectrum of the near-field data is shown for $\varphi$ and $\theta$ polarization. Here the band limitation of the $m$-mode spectrum is obvious. For $|m| > 14$ the magnitude of the modes is small enough to be omitted. This is tested in the next example. The hybrid transformation is carried out three times whereas the $m$-indices are restricted to $-14 \le m \le 14$, $-11 \le m \le 11$, and $-9 \le m \le 9$. The corresponding E- and H-plane far-field patterns are shown in Figures 13 and 14. For the first two simulations no significant influence is evident due to the truncation of the $m$-mode spectrum. For $-9 \le m \le 9$ a degeneration in particular in the backward direction can be seen. This example shows that it is possible to truncate the $m$-mode spectrum to an appropriate value to reduce the computation time without degenerating the accuracy of the transformed far-field pattern.

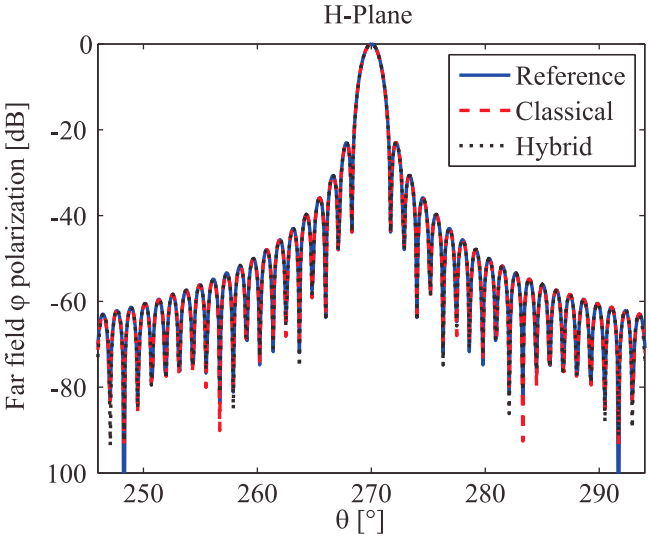


**Figure 18.** Transformed far-field pattern of horn-like antenna at 60 GHz for $m = -141 \ldots 141$, cylindrical measurement $r = 1$ m, $h = 1.2$ m, H-plane cut, $\varphi$ polarization.

### 3.3. Cylindrical Near-Field Measurements

[20] In the next example the applicability of the hybrid transformation algorithm for other "body of revolution" measurement grids than spherical ones shall be emphasized. Therefore a cylindrical measurement grid is chosen as one of the major near-field scanning techniques applied in academia and industry. Electric near fields of a horn-like antenna, aperture size 0.2 m times 0.25 m, have therefore been computed on a cylindrical scanning surface at 60 GHz, to demonstrate the performance of the hybrid multilevel plane wave based transformation algorithm. The scanning surface has a height of 1.2 m and a radius of 1 m, resulting in 216 450 samples for each polarization. The problem has 89 886 unknowns according to the work of *Hansen* [1988]. The $m$-mode spectrum is shown in Figures 15 and 16 for $\varphi$ and z polarization. The processed multilevel measurement setup is described in Table 1 showing the box sizes, maximum number of plane wave samples, and the number of boxes for the different levels.

[21] The transformed E- and H-plane far-field patterns are shown in Figures 17 and 18 and show excellent agreement

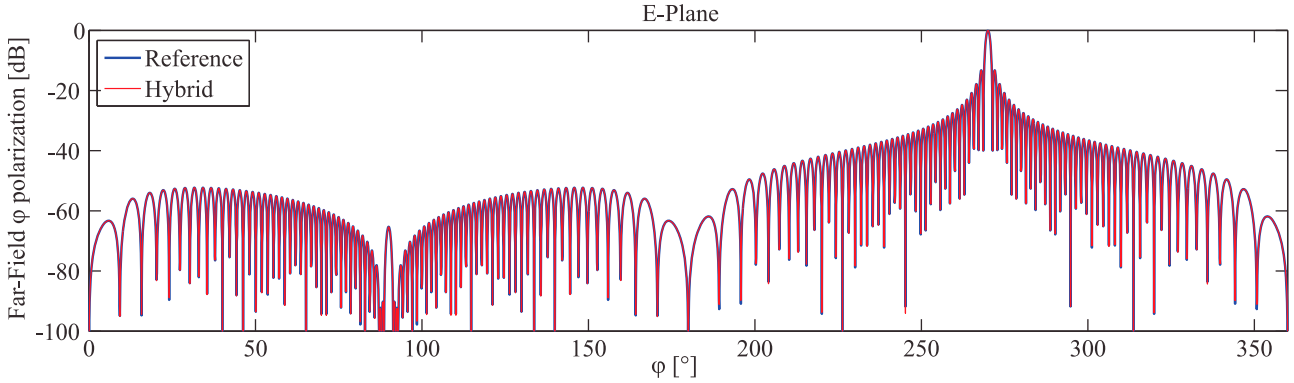


**Figure 17.** Transformed far-field pattern of horn-like antenna at 60 GHz for $m = -141 \ldots 141$, cylindrical measurement $r = 1$ m, $h = 1.2$ m, E-plane cut, $\varphi$ polarization.

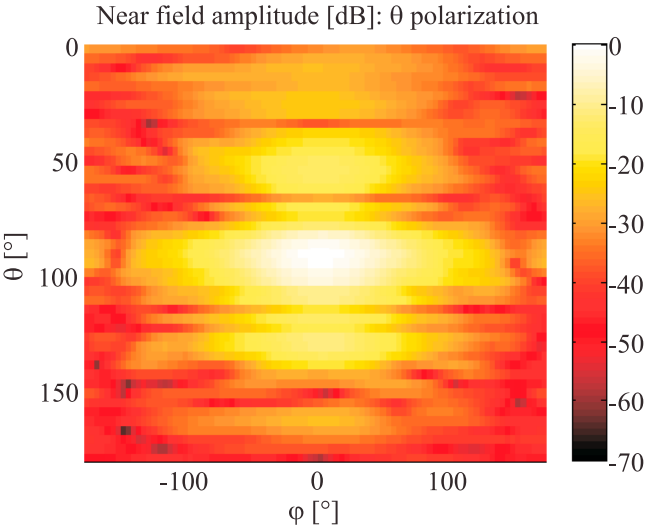


**Figure 19.** Near-field distribution of Kathrein base station antenna type 742 445 at 1.92 GHz, spherical measurement $r$ = 2.715 m, $\theta$ polarization.

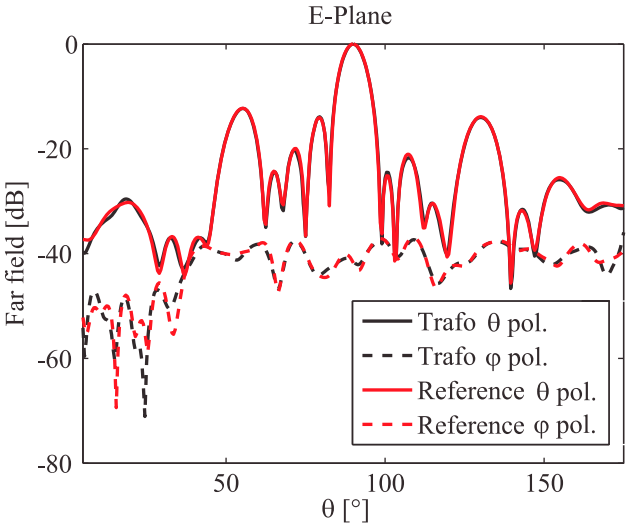


**Figure 21.** Transformed far-field pattern of Kathrein base station antenna type 742 445 at 1.92 GHz, spherical measurement $r$ = 2.715 m, E-plane.

to the reference pattern and the classical transformation algorithm according to the work of *Schmidt and Eibert* [2009]. The H-plane cut is limited to the region of valid angle due to the finite height of the cylindrical measurement grid. The result of the classical transformation algorithm shows similar agreement to the E- and H-plane reference patterns, however the curve for the classical algorithm was omitted in the E-plane cut for clarity. For this example the computer time is 389 min for the classical and 173 min for the hybrid transformation.

## 4. Spherical Near-Field Measurement of Base Station Antenna

[22] A practical measurement of a Kathrein base station antenna of type 742 445 is considered in the next example. The antenna has a height of 1.3 m and is measured at 1.92 GHz using an NSI spherical near-field scanner (Near-field Systems Incorporated, 2010, http://www.nearfield.com). The measurement radius is 2.715 m and 4° step size in $\varphi$ and $\theta$ is applied resulting in 4 140 samples for each probe polarization. An open-ended waveguide probe of type WR430 has been utilized for the measurement. The problem has 2 736 unknowns according to the work of *Hansen* [1988]. The near-field distribution on the measurement sphere as well as the corresponding $m$-mode spectrum are shown in Figures 19 and 20 for the dominant $\theta$ component. The E- and H-plane far-field patterns transformed by the hybrid transformation algorithm are shown in Figures 21 and 22 and are compared to the reference solution obtained by the NSI2000 near-field transformation software.

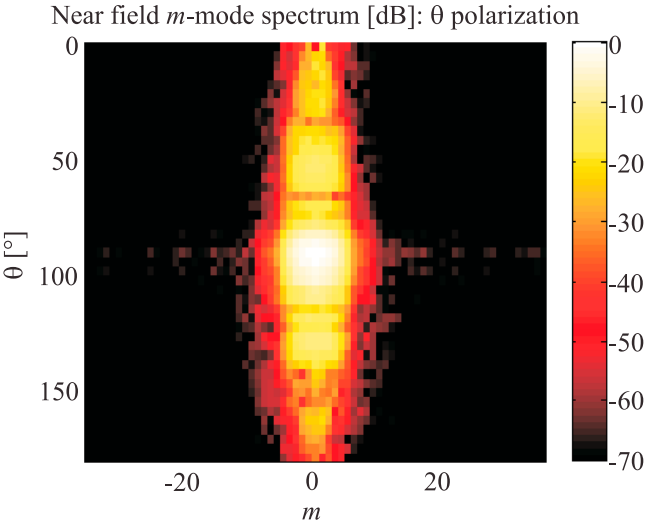


**Figure 20.** The $m$-mode spectrum of Kathrein base station antenna type 742 445 at 1.92 GHz, spherical measurement $r$ = 2.715 m, $\theta$ polarization.

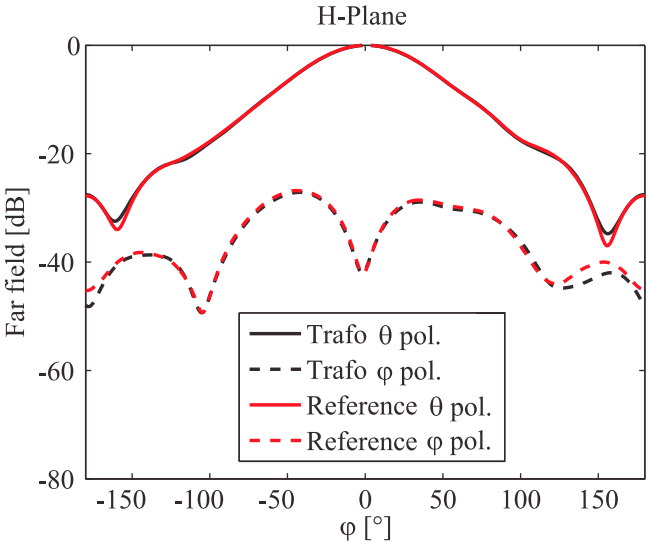


**Figure 22.** Transformed far-field pattern of Kathrein base station antenna type 742 445 at 1.92 GHz, spherical measurement $r$ = 2.715 m, H-plane.

The results are in a very good agreement with each other. Deviations of the order of a couple dB are seen in the E-plane pattern primarily in the pattern nulls below the −30 dB level below the peak. The same applies to the H-plane pattern.

## 5. Conclusion

[23] An efficient hybrid plane wave based near-field far-field transformation technique for "body of revolution" antenna measurement grids and including full probe correction has been presented. The technique preprocesses the measured near-field data by an Inverse Fast Fourier Transform of the measured signals in $\varphi$, and in this way it allows to split the transformation into smaller subsets for the individual azimuthal Fourier modes. Those subsets are then transformed to the far field by the multilevel plane wave based near-field far-field transformation algorithm with its low numerical complexity and its full probe correction capability. The preprocessing allows to speed-up the computation with the complexity remaining the same at the costs of a restriction to measurement grids which are equidistantly sampled in $\varphi$.

[24] **Acknowledgments.** T. Laitinen would like to thank Academy of Finland (decision notification 129055) and German Academic Exchange Service (DAAD) for the financial support of this work. The authors are grateful to KATHREIN-Werke KG, Rosenheim, Germany, for providing the near-field measurement data as well as the NSI transformed far-field pattern.

## References

Abramowitz, M., and I. E. Stegun (1972), *Handbook of Mathematical Functions*, 9th ed., Dover Publ., New York.

Chew, W., J. Jin, E. Michielssen, and J. Song (2001), *Fast and Efficient Algorithms in Computational Electromagnetics*, Artech House, Norwood, Mass.

Coifman, R., V. Rokhlin, and S. Wandzura (1993), The fast multipole method for the wave equation: A pedestrian prescription, *IEEE Antennas Propag. Mag.*, *35*, 7–12.

Hansen, J. E. (Ed.) (1988), *Spherical Near-Field Antenna Measurements*, Peter Peregrinus, London.

Hansen, T. (2009), Complex-point dipole formulation of probe-corrected cylindrical and spherical near-field scanning of electromagnetic fields, *IEEE Trans. Antennas Propag.*, *57*, 728–741.

Jensen, F. (1975), On the probe compensation for near-field measurements on a sphere, *Arch. Elektron. Uebertraeg.*, *29*, 305–308.

Laitinen, T. A. (2008), Double $\phi$-step $\theta$-scanning technique for spherical near-field antenna measurements, *IEEE Trans. Antennas Propag.*, *56*, 1633–1639.

Laitinen, T. A., S. Pivnenko, and O. Breinbjerg (2005), Odd-order probe correction technique for spherical near-field antenna measurements, *Radio Sci.*, *40*, RS3009, doi:10.1029/2004RS003063.

Laitinen, T. A., S. Pivnenko, J. M. Nielsen, and O. Breinbjerg (2010), Theory and practice of the FFT/matrix inversion technique for probe-corrected spherical near-field antenna measurements with high-order probes, *IEEE Trans. Antennas Propag.*, *58*, 2623–2631.

Larsen, F. H. (1977), Probe correction of spherical near-field measurements, *Electron. Lett.*, *13*, 393–395.

Pogorzelski, R. J. (2008), A method of achieving full correction of an arbitrary probe in spherical near-field measurement, in *IEEE AP-S International Symposium and USNC/URSI National Radio Sci. Meeting*, San Diego, Calif., 5–11 July.

Saad, Y. (2003), *Iterative Methods for Sparse Linear Systems*, 2nd ed., Soc. for Ind. and Appl. Math., Philadelphia.

Schmidt, C. H., and T. F. Eibert (2009), Multilevel plane wave based near-field far-field transformation for electrically large antennas in free-space or above material halfspace, *IEEE Trans. Antennas Propag.*, *57*, 1382–1390.

Schmidt, C. H., M. M. Leibfritz, and T. F. Eibert (2008), Fully probe-corrected near-field far-field transformation employing plane wave expansion and diagonal translation operators, *IEEE Trans. Antennas Propag.*, *56*, 737–746.

Schmidt, C. H., T. A. Laitinen, and T. F. Eibert (2010), Fast Fourier Transform preprocessing for accelerated plane wave based spherical near-field far-field transformation, in *URSI International Symposium on Electromagnetic Theory*, Berlin, 16–19 August.

Wacker, P. F. (1974), Near-field antenna measurements using a spherical scan: Efficient data reduction with probe correction, *IEE Conf. Publ.*, *113*, 286–288.

Yaghjian, A. (1986), An overview of near-field antenna measurements, *IEEE Trans. Antennas Propag.*, *34*, 30–45.

Yaghjian, A. D., and R. C. Wittmann (1985), The receiving antenna as a linear differential operator: Application to spherical near-field scanning, *IEEE Trans. Antennas Propag.*, *33*, 1175–1185.

T. F. Eibert and C. H. Schmidt, Lehrstuhl für Hochfrequenztechnik, Technische Universität München, Arcisstr. 21, D-80333 Munich, Germany. (eibert@tum.de; carstenschmidt@tum.de)

T. A. Laitinen, Aalto University School of Electrical Engineering, Department of Radio Science and Engineering, PO Box 13000, FI-00076 Espoo, Finland. (tommi.laitinen@aalto.fi)